Resistive–ideal transition of pressure-driven instabilities in current-carrying plasmas beyond the Suydam criterion

F. Ebrahimi, S. C. Prager, and C. R. Sovinec
University of Wisconsin—Madison, Madison, Wisconsin 53706

(Received 14 January 2002; accepted 8 April 2002)

The linear magnetohydrodynamics stability of local and global resistive pressure-driven instabilities is examined computationally in a cylinder. Both instabilities are resistive from beta values of zero up to several times the Suydam limit. Both transition to ideal modes at higher beta values. No sudden change in growth rate occurs at the Suydam limit. The global pressure-driven modes, of tearing parity, will likely be important in high beta plasmas, such as obtained in the reversed field pinch. © *2002 American Institute of Physics.* [DOI: 10.1063/1.1481860]

The linear stability of ideal and resistive pressure-driven interchange modes is an old subject that has received extensive analysis. Its relevance today is somewhat heightened, as experiments with unfavorable magnetic curvature, such as reversed field pinches (RFP) and stellarators, are operating with pressure at or above the ideal interchange stability limit. In stellarators beta values above the Mercier limit are obtained in experiment, with no observation of instability.[1] The investigation of global resistive modes have been examined in stellarators in currentless equilibria applicable to the Heliotron DR device.[2] In the RFP, control of the current density profile has succeeded in substantially reducing current-driven tearing instability and increasing beta to the point that pressure-driven modes may begin to be consequential.[3] In this paper we examine the behavior of the linear resistive interchange instability in current-carrying cylindrical plasmas, as beta varies from less than the ideal stability (Suydam) limit to much larger than the ideal limit.

The ideal interchange instability in a cylinder has been examined in some detail, following the calculation by Suydam that a localized pressure-driven instability in a bad curvature region, is excited if the stability parameter $D_S = -(8\pi p'/r)(q/B_z q')^2|_{r_s} > 0.25$,[4] where q is the safety factor, p is the pressure and $(\,)' = d/dr$. Subsequently, the dependence of the analytic growth rate on D_S (in the limit of large wave number, k) has been treated by several authors.[5,6] In many of these treatments the inertial term is included in a layer around the resonant surface only. The eigenfunction solution in the outer region is matched to that obtained in the layer.[7–9] The result is that the growth rate depends on D_S (which is proportional to beta) as $\gamma_{\max} \approx C \exp(-2\pi/\sqrt{\sigma})$, where $\sigma = D_S - 0.25$. Thus, the growth rate is exponentially small near the ideal limit ($D_S = 0.25$), becoming large for D_S values well above this limit. Numerical values for the growth rate of ideal interchange modes have also been obtained in a diffuse linear pinch.[10,11]

The addition of small resistivity defeats the shear stabilization and resistive interchange modes become always unstable in a cylinder.[12] Matching the outer solution to a layer that includes resistivity yields an analytical growth rate that scales with Lundquist number, S, as $\gamma \sim S^{-1/3}$.[13] Numerical studies of the growth rate have been accomplished using eigenmode analysis (matrix shooting).[14–16]

In the present work, we employ initial value computation to evaluate the growth rate and radial structure, for an arbitrary wave number, of the resistive pressure-driven instability. We find two results. First, for a rather wide range of beta, from zero to several times the Suydam limit, the high-k interchange mode is resistive. It is resistive in its radial structure (which results in reconnection), and its growth rate, which is small and scales as $S^{-1/3}$ at low D_S, and more weakly with S as D_S increases. The instability transitions to an ideal mode at very high beta values (D_S), several times the Suydam limit. Only at these very high beta values is the

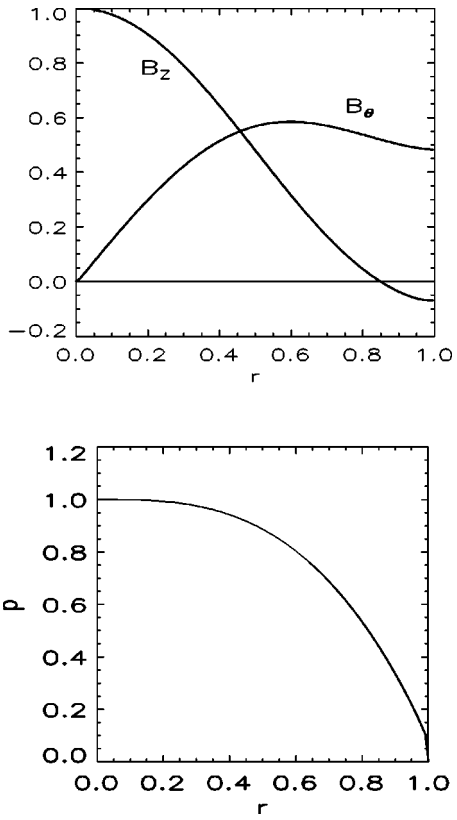

FIG. 1. Equilibrium magnetic field and pressure profiles (B_Z, B_θ, p).

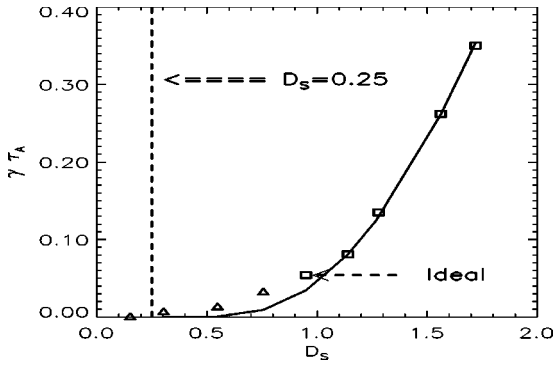

FIG. 2. The growth rate, $\gamma\tau_A$, of the $m=1$, $k=10.5$ mode vs D_S. $S=10^6$, $\theta_0=1.6$, $\alpha=4$, $\delta=3$, $p_1=0.9$. The triangles are computational results corresponding to resistive modes and the square boxes correspond to pure ideal modes. The solid line is the analytical growth rate of ideal interchange modes. The transition from resistive to ideal interchange modes occurs at high $D_S\sim1.0$. The dashed vertical line is the Suydam limit.

mode ideal in its radial structure and its growth rate (which becomes independent of S and scales with D_S as described by ideal MHD). Second, we find that for the RFP global pressure-driven modes are important. These modes transition from resistive to ideal as beta increases, similar to that of the interchange.

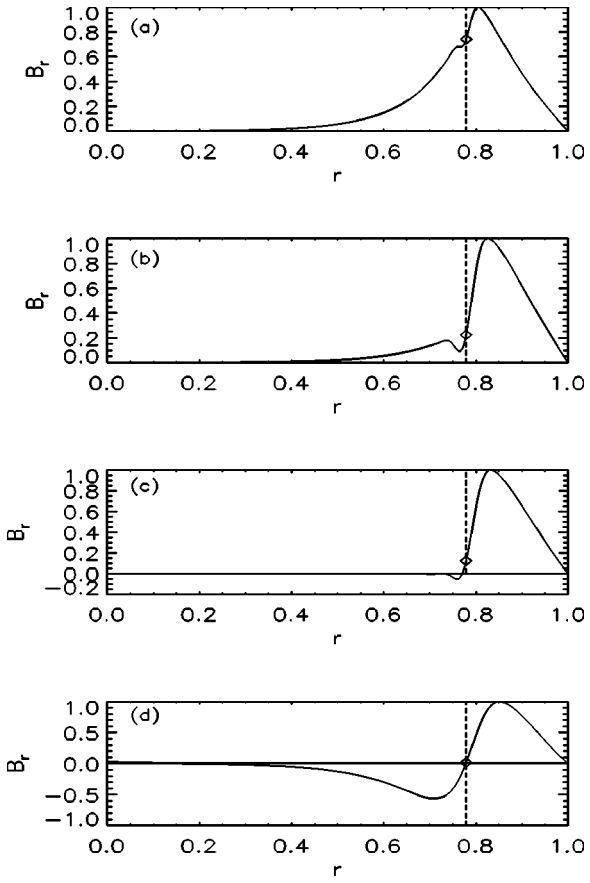

FIG. 3. Radial magnetic field magnitude vs radius for (a) $D_S=0.23$, $\gamma\tau_A=6.5\times10^{-3}$, (b) $D_S=0.756$, $\gamma\tau_A=3.3\times10^{-2}$, (c) $D_S=0.95$, $\gamma\tau_A=5.4\times10^{-2}$, (d) $D_S=1.72$, $\gamma\tau_A=0.35$. For all cases $S=10^6$, $m=1$, $k=10.5$.

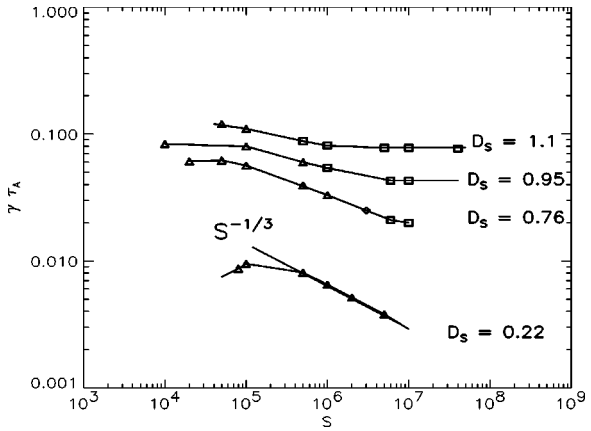

FIG. 4. Growth rate scaling of localized interchange mode $m=1$, $k=10.5$, with Lundquist number S, for various values of D_S. At low D_S (<0.25) this scaling is resistive and at high D_S (high β) is ideal.

The three dimensional nonlinear DEBS code[17] is used to solve the following set of compressible resistive MHD equations in cylindrical geometry in the linear regime:

$$\frac{\partial\overline{A}}{\partial t}=S\overline{V}\times\overline{B}-\eta\overline{J},$$

$$\rho\frac{\partial\overline{V}}{\partial t}=-S\rho\overline{V}\cdot\nabla\overline{V}+S\overline{J}\times\overline{B}+\nu\nabla^2\overline{V}-S\frac{\beta_0}{2}\nabla P,$$

$$\overline{B}=\nabla\times\overline{A},\quad \overline{J}=\nabla\times\overline{B},$$

$$\frac{\partial P}{\partial t}=-S\nabla\cdot(P\overline{V})-S(\gamma-1)P\nabla\cdot\overline{V},$$

where time and radius are normalized to resistive diffusion time $\tau_R=4\pi a^2/c^2\eta_0$ and minor radius a, $S=\tau_R/\tau_A$ is the Lundquist number, ν is the viscosity coefficient, which measures the ratio of characteristic viscosity to resistivity (the magnetic Prandtl number), and $\beta_0=8\pi P_0/B_0^2$ is the beta

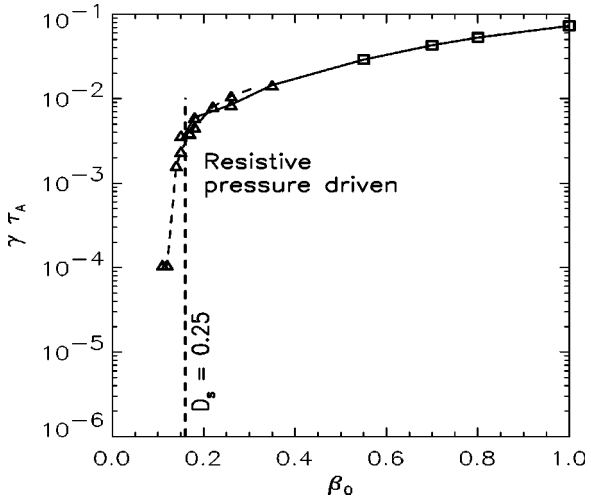

FIG. 5. Growth rate of low-k pressure-driven mode, $m=1$ $k=1.8$ mode vs β_0. The triangles denote resistive modes and the square boxes denote pure ideal modes. Some of the points are computed at $S=10^4$ (dashed curve), and while some are at $S=10^5$ (solid curve).

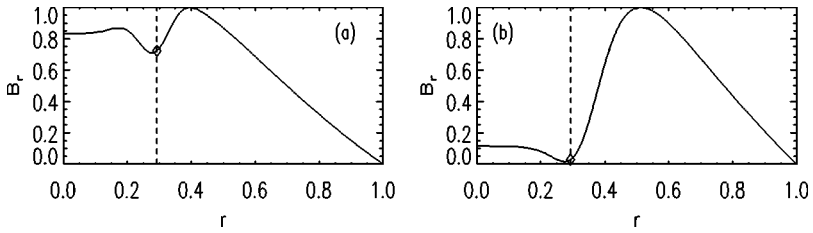

FIG. 6. Radial magnetic field B_r vs radius for global modes ($m=1$, $k=1.8$) at $S=10^5$ for (a) $D_S=0.24$, $\gamma\tau_A=3.4\times10^{-3}$, (b) $D_S=1.3$, $\gamma\tau_A=7.3\times10^{-2}$.

normalized to the axis value. The mass density ρ is assumed to be uniform in space and time. The equations are fully compressible and describe both shear and compressional Alfvén waves, as well as resistive instabilities. To resolve the ideal and resistive interchange modes in the linear computation, the maximum timestep has been examined for convergence. The growth rate solutions are converged in timestep and spatial resolution to the level of 2% and 1%, respectively. The code uses the finite difference method for the radial coordinate.

To isolate the pressure-driven modes, an equilibrium which is stable to resistive current-driven modes is chosen (by the Δ' criterion). The equilibrium parallel current profile and pressure profile are $\lambda(r)=J\cdot B/B^2=2\theta_0(1-r^\alpha)$ and $p(r)=p_0(1-p_1r^\delta)$, respectively, where α, θ_0, δ, p_0 and p_1 are free constants. Other equilibrium quantities can be computed from the θ and z components of $\nabla\times\bar{B}=\lambda(r)\bar{B}+\beta_0\bar{B}\times\nabla p(r)/2B^2$ (see Fig. 1).

First, we examine highly localized interchange modes by choosing modes with high axial wave number, k. The dependence of the growth rate on $D_S=-(8\pi p'/r)(q/B_zq')^2|_{r_s}$ is shown in Fig. 2. The mode selected (azimuthal mode number $m=1$, $k=10.5$) is resonant at $r/a=0.78$. We see that the growth rate is always nonzero and increasing with D_S, but follows the analytical ideal value only at $D_S>1.0$. The growth rate at lower D_S values is much greater than the ideal growth rate. It increases smoothly through the Suydam limit ($D_S=0.25$), which plays no role for resistive instability. As expected, the growth rate depends on D_S only, rather than its constituents, β_0 or magnetic shear, separately.

The radial structure of instability also indicates that a transition from a resistive to ideal interchange mode occurs at $D_S\sim1.0$ (for this particular m, k and S). Ideal and resistive instabilities can be distinguished by the magnitude of the radial magnetic field B_r. The radial field is nonzero at the resonant surface only for a resistive mode. We see that the mode structure is resistive for $D_S<0.9$ [Figs. 3(a) and 3(b)] and ideal for $D_S>0.9$ [Figs. 3(c) and 3(d)], in agreement with the growth rates of Fig. 2.

The transition from resistive to ideal modes is also evident in the S dependence of the growth rate γ (Fig. 4). At low D_S, γ scales as $S^{-1/3}$ (resistive scaling), whereas at very high D_S, γ is roughly independent of S (ideal scaling). The D_S value at which the mode transitions from a resistive to an ideal mode depends upon S. The transition value for D_S decreases with S. This can be inferred from Fig. 4. The triangles are resistive modes (from the radial structure) and the square boxes are ideal. For values of S (10^6-10^7) of the present experiments, the transition occurs at $D_S\sim0.7-1.0$ (or $\beta_0\sim40-60\%$) well above experimental beta values.

High-k localized modes can be stabilized by finite Larmor radius effects.[8,18] Thus, global, low-k pressure-driven modes may be more important for the RFP. The ideal stability of global pressure-driven modes have been examined in the past and it has been shown that these modes become unstable with the violation of Suydam criterion as well and have kink-like behavior.[11] Prior calculation of the growth rate for the resistive global pressure-driven modes also show an explicit dependence on the local parameter, D_S (as well as the global parameters).[12] Here, we have examined the growth rate and radial structure of global modes, and find that they also display a transition from resistive to ideal instability as beta increases. The growth rate for the $m=1$, $k=1.8$ mode is shown in Fig. 5. The triangles correspond to resistive modes (as judged from the radial structures), while the boxes correspond to ideal modes. The mode is unstable at low beta

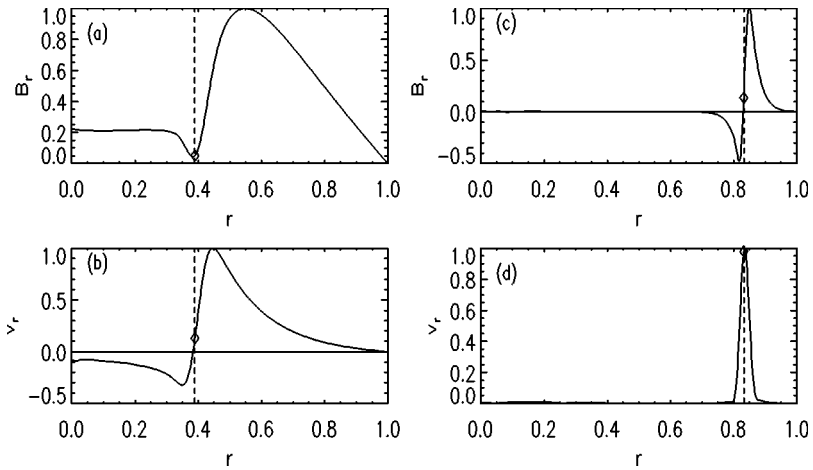

FIG. 7. Radial magnetic field (B_r) and radial velocity (v_r) eigenfunctions for global kink ($m=1$, $k=2$) and localized interchange ($m=1$, $k=45$) modes in the ideal limit ($S=10^6$, $D_S=0.9$). (a) B_r for $k=2$, (b) v_r for $k=2$, (c) B_r for $k=45$, (d) v_r for $k=45$.

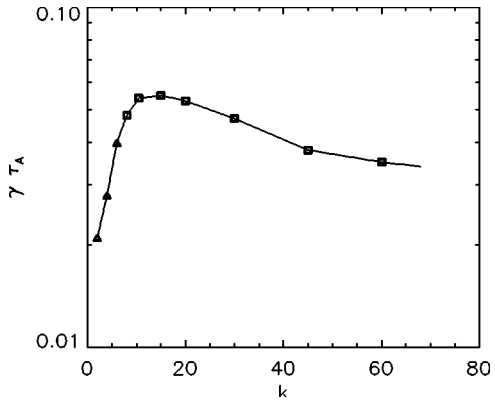

FIG. 8. Wave number spectrum of ideal pressure-driven modes at $D_s \sim 1.0$, $S = 10^6$. Triangles denote modes with a radial structure with tearing mode parity; boxes denote interchange parity.

values (less than the Suydam limit) and transitions to ideal modes at high beta (several times the Suydam limit). The radial structure for low and high D_S values (Fig. 6) shows the change from a resistive to an ideal structure. These modes differ from the localized modes in their parity. The global mode structure for the radial magnetic and velocity fields [Figs. 7(a) and 7(b)] show tearing mode parity (B_r even about the resonant surface, v_r odd). The parity is opposite for the localized interchange modes [Figs. 7(c) and 7(d)]. The k spectrum of the growth rate of all pressure-driven modes (Fig. 8) illustrates the transition from tearing parity modes (depicted by triangles) to interchange parity (boxes) as k increases. We also observe that the growth rate for the global modes is about equal to that of the localized interchange.

The resistive–ideal transition of the localized modes is similar to that calculated for the stellarator.[2] However, there are significant differences between the behavior of global modes. In the currentless stellarator, the global, low-k modes have interchange parity and do not display a transition to a distinct ideal structure. In contrast, for the current-carrying plasmas examined here, modes with tearing parity are the most unstable and evolve from resistive to ideal at high beta.

In summary, motivated by the advance of present day experiments toward high beta regimes, we have revisited the behavior of linear local and global resistive pressure-driven MHD instabilities over a wide range of beta and resistivity (Lundquist number). We find that the Suydam criterion is not very relevant, in agreement with an earlier analytical calculation of ideal growth rates. The localized interchange is resistive (in growth rate and radial structure) at beta values up to several times the Suydam limit, transitioning to an ideal mode at extremely high beta. No sudden changes in growth rate occur at the Suydam limit. This result may be consistent with the apparent absence of localized instability onset in experiments operating at or above the Suydam (or Mercier) stability limit.[1] For the RFP, we find that global pressure-driven modes (of tearing spatial parity) are equally unstable and have a similar transition from resistive to ideal as beta increases. Since the localized modes are more subject to stabilization mechanisms beyond MHD (such as finite Larmor radius stabilization), the global modes will likely be more influential in the reversed field pinches at high beta. In future studies we will examine the nonlinear behavior of these instabilities.

ACKNOWLEDGMENTS

We are happy to acknowledge useful discussions with Chris Hegna and John Wright.

[1] S. Okamura, K. Matsuoka, K. Nishimura *et al.*, in *Proceedings of the 15th International Conference on Plasma Physics and Controlled Nuclear Fusion Research* (International Atomic Energy Agency, Vienna, 1995), Vol. 1, p. 381.
[2] K. Ichiguchi, Y. Nakamura, M. Wakatani, N. Yanagi, and S. Morimoto, Nucl. Fusion **29**, 2093 (1989).
[3] J. Sarff, N. Lanier, S. C. Prager, and M. R. Stoneking, Phys. Rev. Lett. **78**, 62 (1997).
[4] B. R. Suydam, in *Proceedings of the 2nd United Nations International Conference on the Peaceful Uses of Atomic Energy*, Geneva, 1958, Vol. 31, p. 152.
[5] H. Grad, Proc. Natl. Acad. Sci. U.S.A. **70**, 3277 (1973).
[6] Y. P. Pao, Nucl. Fusion **14**, 25 (1974).
[7] R. M. Kulsrud, Phys. Fluids **6**, 904 (1963).
[8] T. E. Stringer, Nucl. Fusion **15**, 125 (1975).
[9] S. Gupta, C. C. Hegna, and J. D. Callen, "Violating Suydam criterion produces feeble instabilities," submitted to Phys. Plasmas.
[10] J. P. Goedbloed and H. J. Hagebeuk, Phys. Fluids **15**, 1090 (1972).
[11] J. P. Goedbloed and P. H. Sakanaka, Phys. Fluids **17**, 908 (1974).
[12] B. Coppi, J. M. Greene, and J. L. Johnson, Nucl. Fusion **6**, 101 (1966).
[13] H. P. Furth, J. Killeen, and M. N. Rosenbluth, Phys. Fluids **6**, 459 (1963).
[14] J. P. Freidberg and D. W. Hewett, J. Plasma Phys. **26**, 177 (1981).
[15] D. Merlin, S. Ortolani, R. Paccagnella, and M. Scapin, Nucl. Fusion **29**, 1153 (1989).
[16] D. H. Liu, Nucl. Fusion **37**, 1083 (1997).
[17] D. D. Schnack, D. C. Barnes, Z. Mikic, D. S. Harned, and E. J. Caramana, J. Comput. Phys. **70**, 330 (1987).
[18] M. N. Rosenbluth and N. Krall, Nucl. Fusion Suppl. **A1**, 143 (1962).